What ocean biogeochemical models can tell us about bottom-up control of ecosystem variability

Journal:	*ICES Journal of Marine Science*
Manuscript ID:	ICESJMS-2010-160.R1
Manuscript Types:	Symposium Article
Date Submitted by the Author:	10-Dec-2010
Complete List of Authors:	Gnanadesikan, Anand; NOAA Geophysical Fluid Dynamics Lab, Oceans and Climate Group Dunne, John; NOAA Geophysical Fluid Dynamics Lab, Climate and Ecosystems Group John, Jasmin; NOAA Geophysical Fluid Dynamics Lab, C; NOAA Geophysical Fluid Dynamics Lab, Climate and Ecosystems Group
Keyword:	biome extent, climate models, nutrient limitation, salinity, size structure, spring bloom

What ocean biogeochemical models can tell us about bottom-up control of ecosystem variability

Anand Gnanadesikan, John P. Dunne and Jasmin John

Processes included in earth system models amplify the impact of climate variability on phytoplankton biomass and thus on upper trophic levels. Models predict much larger relative interannual variability in large phytoplankton biomass compared with total phytoplankton biomass, supporting the goal of better constraining size-structured primary production and biomass from remote sensing. The largest modeled variability in annually-averaged large phytoplankton biomass is associated with changes in the areal extent of relatively productive regions. Near the equator, changes in areal extent of the high-productivity zone are driven by large-scale shifts in nutrient fields as well as changes in currents. Along the poleward edge of the subtropical gyres, changes in physical mixing dominate. Finally, models show that high-latitude interannual variability in large phytoplankton biomass is highest during the spring season. Mechanisms for producing such variability differ across biomes with internal ocean processes such as convection complicating efforts to link ecosystem variability to climate modes defined using sea surface temperature alone. In salinity-stratified subpolar regions, changes in bloom timing driven by salinity can produce correlations between low surface temperatures and high productivity, supporting the potential importance of using coupled atmosphere-ocean reanalyses rather than simple forced ocean reanalyses for attributing past ecosystem shifts.

Keywords: Biome extent, climate models, nutrient limitation, salinity, size structure, spring bloom

Anand Gnanadesikan, John P. Dunne and Jasmin John, NOAA Geophysical Fluid Dynamics Laboratory, 201 Forrestal Road, Princeton University, Princeton, NJ 08540 USA

P: 1-609-987-5062 E: anand.gnanadesikan@noaa.gov

Introduction

As Earth System Models are developed for projecting biogeochemical changes under global warming, a natural question that arises is whether they will be useful for projecting changes in fisheries production, particularly those driven by bottom-up changes in the productivity or species composition associated with phytoplankton. One potential test is whether such models can simulate interannual variability. Variability in the stocks of a number of species has been reported on interannual to decadal scales and linked to climate modes such as the Pacific Decadal Oscillation and North Atlantic Oscillation. For example, basin scale modes in the Pacific have been linked to variability in such species as salmon in the Pacific Northwest (Mantua et al., 1997), walleye pollock in the Bering Sea (Hunt et al., 2008), Japanese eel in the Kuroshio region (Sugimoto et al., 2001; Kimura and Tsukamoto, 2006) and sardine and anchovy in the Peru Current (Chavez et al., 2003).

Physical climate models may be able to address proposed mechanisms for interannual changes in stocks such as temperature impacts on spawning times and locations (e.g. Genner et al., 2004), changes in the frequency of warm events such as those associated with coral bleaching (Glynn and DeWeerdt, 1991), changes in the frequency of cold events associated with wintertime mortality (Hare et al. 2009), or changes in the advective pathways for larval transport (e.g. Sugimoto et al. 2001, Kimura and Tsukamoto, 2006). While not deprecating the potential importance of such direct physical forcing for individual species, this paper focuses on

simulations of primary productivity provided by a new generation of Earth System Models. For many years, fisheries oceanographers have recognized that the details of primary production such as the timing of blooms (Hjort, 1914; Cushing, 1990) or differences in phytoplankton community structure (Ryther, 1969) could explain variations in ecosystems over time and space. We examine whether the large-scale Earth System Models used for projecting climate change represent such aspects of the primary productivity signal that both observations and theory suggest vary significantly from year to year. Additionally, we investigate what models can tell us about the magnitude of such variability and about the physical processes underlying it. We show that the current generation of Earth System Models do simulate drivers of interannual ecosystem variability beyond annually averaged changes in biomass. These drivers include changes in the areal extent of productive regions, changes in the timing of blooms and changes in the concentration of large phytoplankton.

Variability in the abundance of large phytoplankton is especially important, as their grazers have long been thought to represent the key pathway by which energy is transferred to higher trophic levels, leading to the classic statement that "all fish is diatoms" (Bigelow, 1926). In upwelling regions rich in macronutrients, larger phytoplankton dominate and recycling of nutrient is inefficient (Dugdale and Goering, 1968). In weakly productive subtropical gyres where macronutrients are at low levels, small picoplankton have been found to account for most of the primary productivity (Platt et al., 1983) and recycling of nutrients is high. This leads to less variation in total biomass across biomes than would be expected from the differences in nutrient supply, as well as less spatial variability in small phytoplankton biomass than large phytoplankton biomass. Agawin et al. (2000) noted that the concentration of large plankton showed 5-6 orders of magnitude variation in mesocosm experiments, while small plankton

biomass concentrations varied over about 2 orders of magnitude. Similar results for remotely sensed concentrations of large and small particle concentrations were recently presented by Kostadinov et al. (2009) and for primary productivity by Uitz et al. (2010). The idea that such differences in size structure of primary producers, translated up the food web, are responsible for the differences in fisheries production between ecosystems goes back at least to Ryther (1969). However, since in-situ time series of size-fractionated productivity and biomass do not exist in most of the regions where large relative variability is seen, it is worth examining whether models can be used to characterize the variability of large phytoplankton on global scales.

The current generation of ocean biogeochemical and earth system models combine information about physical forcing, chemical cycling, phytoplankton physiology and ecological structure to simulate the response of lower trophic levels to climate variability and change (Six and Meier-Reimer, 1996; Aita et al., 2003, 2007; Moore and Doney, 2004; Aumont and Bopp, 2006; Galbraith et al., 2010; Kishi et al., 2010). Built around ocean circulation models that use the conservation of heat, mass, salt and momentum to solve for a physical circulation consistent with surface forcing, such models can be forced by datasets based on atmospheric reanalysis products (Griffies et al., 2009) to produce retrospective estimates of biological activity. Alternatively, they can be embedded in fully coupled ocean-atmosphere circulation models to estimate how ocean ecosystems could change in the future as a result of changes in greenhouse gasses (e.g. Steinacher et al., 2010).

This paper examines what such models can tell us about the potential for quantitatively and mechanistically linking variability in primary productivity to climate variability and change. Section 2 describes how the Tracers of Ocean Productivity with Allometric Zooplankon (TOPAZ) model used in the NOAA Geophysical Fluid Dynamics Laboratory's Earth System Model

(Sarmiento et al., 2010; Dunne et al., 2010) represents key ideas about phytoplankton size structure and describes two physical circulation models in which it has been implemented. Section 3 shows output from these simulations, quantifying the dominance of large phytoplankton variability over much of the ocean, further highlighting the importance of changes in areal extent of biomes, and also considering the impact of interannual variability in bloom timing. Section 4 expands on the mechanisms by which tropical variability on interannual time scales changes the areal extent of the oligotrophic tropical gyres. Section 5 expands on the mechanisms driving interannual variability in springtime productivity in four North Pacific regions. Section 6 concludes the paper by examining the implications of our results for observational strategies in characterizing fisheries and for developing new retrospective modeling analyses.

2. The models

a.) Size structure in the GFDL ecosystem models

We begin by describing the ecosystem model used in one Earth System Model, the Geophysical Fluid Dynamics Lab's TOPAZ code. A preliminary description of the TOPAZ biogeochemical model is presented in Dunne et al. (2010). We therefore focus on how the model represents the response of phytoplankton biomass to varying environmental conditions and how this differs between large and small phytoplankton.

Like other biogeochemical models of intermediate complexity, TOPAZ divides the phytoplankton community into a small number of functional groups which react differently to light and nutrient limitation. The growth rate of a given class of phytoplankton is given by

$$\mu = \frac{P^C_{max}}{1+\zeta} e^{kT}\ min(\ Lim_N, Lim_P, Lim_{Fe}\ )* Lim_{Irr} \quad (1)$$

Where P^C_{max} is a maximum carbon assimilation rate in 1/s, ζ is a cost of biosynthesis (set to 0.1), k is the Eppley temperature coefficient (0.063/K), T is the temperature in K, and $Lim_{N,P,Fe,Irr}$ refer to limitation terms for nitrogen, phosphorus, iron and light respectively. Phytoplankton are then limited by the temperature, whatever nutrient is most limiting, and by light.. Nitrogen limitation is given by

$$Lim_N = max\left(\frac{NO_3}{K_{NO3} + NO_3(1 + NH4 / K_{NH4})}, \frac{NH_4}{K_{NH4} + NH_4}\right) \quad (2)$$

following Frost and Franzen (1992), with NO3 and NH4 referring to the ambient nitrate concentrations, so that nitrate limitation becomes less important in the presence of ammonia. The physiological nutrient limitation terms $Lim_{P,Fe}$ are determined from the actual N:P and Fe:P cellular quotas which change through a complicated process described in detail in Dunne et al. (2010) based on the theoretical work of Klausmeier et al. (2004). As these terms turn out to be of minor importance in the regions presented below, we refer the reader to Dunne et al., (2010) for a complete description of how they work and do not discuss them further.

Light limitation is parameterized as

$$Lim_{Irr} = 1 - exp(-\alpha\theta I / P^C_N\ ) \quad (3)$$

In this equation, α is the initial slope of the chlorophyll-a specific photosynthesis-light response curve (units of molC/(mol chl*J/m^2)) and thus governs how rapidly photosynthesis (relative to chlorophyll) increases at low light levels assuming constant chlorophyll. θ is a chlorophyll to carbon ratio (mol chl/mol C), I is the incoming solar radiation in W/m^2 and

$P_N^C = P_{max}^C e^{kT}\ min(\ Lim_N, Lim_P, Lim_{Fe}\ )$ is the nutrient-limited carbon assimilation rate in 1/s. In a modified version of the formulation proposed by Geider et al. (1997) we then let

$$\theta = \theta_{min}\ min(\ Lim_N, Lim_P, Lim_{Fe}\ ) + \frac{\theta_{max} - \theta_{min}}{1 + \alpha(\ \theta_{max} - \theta_{min}\ )I / 2P_N^C} \qquad (4)$$

so that as nutrients increase (or light decreases), the chl:C level ratio increases to match the increased need for light harvesting efficiency. This means that variations in chlorophyll concentration can be driven by variations in the available light (say as a result of changing insolation or mixed layer depth) which will not necessarily reflect changes in biomass. In contrast to the version of the code used in Sarmiento et al.. (2010), we do not let θ_{max} depend on iron limitation. As discussed in Galbraith et al., (2010) the primary impact of neglecting such dependence is seen in the North Atlantic, where high levels of iron allow for an earlier spring bloom and faster drawdown of surface nutrients.

The concentration of phytoplankton is determined by a balance between the growth rate and grazing rate. The representation of grazing in TOPAZ is based on the work of Dunne et al. (2005), in which the equation governing a given class of phytoplankton biomass is

$$\frac{\partial P}{\partial t} = \mu_P P - \lambda \left(\frac{P}{P_*}\right)^a P \qquad (5)$$

where P is the concentration of some class of phytoplankton, μ_P is a growth rate, λ is a grazing rate, P_* is a scale concentration for grazing and a is the grazing parameter (a=1 for classic logistic growth). . TOPAZ uses the Dunne et al. (2005) values of P*=1.9 mmol C/m^3 and $\lambda = 0.19e^{kT} / 86400s$. If growth and grazing are approximately in balance, then

$$P \approx \left(\frac{\mu_P}{\lambda}\right)^{1/a} P_* \qquad (6)$$

Different groups of plankton may thus differ in how they are controlled by nutrients, or by how tightly they are controlled by grazing.

TOPAZ distinguishes between three functional groups.

1. Small plankton: Meant to represent nanoplankton such as Synechecoccus and prochlorococcus, this class of phytoplankton has relatively low half-saturation coefficients for iron (5 nM), ammonia (0.2 μM), phosphorus (0.2 μM) and nitrate (2.0 μM). P^C_{max} is set to 2.0 x 10^{-5} /s. The grazing exponent *a* is set to 1 following Dunne et al. (2005). This class of phytoplankton is thus weakly limited by nutrients, but strongly limited by grazing.

2. Large plankton: Meant to represent green algae, diatoms and other large phytoplankton, this class of plankton has half-saturation constants for uptake that are three times that for small phytoplankton, than small phytoplankton, and the ability to store iron internally. The grazing exponent for large phytoplankton *a*=1/3 following Section 5.1 of Dunne et al. (2005) (this value is also used in Galbraith et al., 2010). Thus while the large plankton require much higher levels of nutrient to realize their maximum growth rate, their concentration actually goes as the *cube* of that growth rate because they are less tightly limited by grazing. The fraction of large phytoplankton taken to be diatoms is given by

$$F_{diat} = \frac{SiO4}{K_{Si} + SiO4_*} \quad (7)$$

With K_{si}=3 mmol/m^3. so that silicate limitation results in reducing the diatom fraction.

3. Diazotrophs: Meant to represent organisms such as Trichodesmium which fix nitrogen from N_2, these organisms require four times as much iron as the small plankton and have a maximum growth rate 40% of the small plankton. The grazing exponent is the same as for large

phytoplankton. However, while diazotrophs play a critical role in maintaining the nitrogen inventory of the ocean they represent a relatively small fraction of biomass in our simulations, and their dynamics will thus be effectively ignored for the remainder of the paper.

Considering then only the scaling between large and small phytoplankton, then, we can find two separate regimes. When nutrients or light are extremely limiting, (for example when $NH4 << K_{NH4}^{sm} < K_{NH4}^{Lg}$) then an increase in the limiting nutrient result in the same *relative* change in the growth rate for small and large phytoplankton. However, because of the different grazing laws, this will result in a proportional increase in the concentration of small phytoplankton $S \propto NH4$, but a much larger relative change in the concentration of large phytoplankton $L \propto S^3 \propto NH4^3$. When the concentration of the most limiting nutrient is higher than the half-saturation constant for the small phytoplankton $K_{NH4}^{sm} < NH4$, relative changes in growth rate are bigger for large phytoplankton than for small phytoplankton, so that the ratio of large to small phytoplankton follows an even higher power law. Thus, in general, we expect to find more variability in large phytoplankton concentration than in small phytoplankton concentration.

b.) Ocean-ice model

The ocean-ice model used in these simulations is the ocean-ice component of the GFDL CM2.1 global coupled climate model (Delworth et al., 2006). The model is configured with 50 vertical layers with thicknesses ranging from 10m over the top 200m to a maximum thickness of 250m at 5500m depth. The meridional resolution is 1 degree while the zonal resolution varies from 1 degree in mid-latitudes to 1/3 degree at the equator. North of 65 degrees a tripolar grid is

employed to avoid the polar singularity. Up-to-date parameterizations of mixed layer dynamics, isopycnal mixing, advection by subgridscale eddies, bottom topography and bottom flows and lateral viscosity are included (Griffies et al., 2005; Gnanadesikan et al. 2006). Both the dynamics and thermodynamics of five thickness classes of sea ice are simulated.

Surface forcing is set using the Coordinated Ocean-ice Reference Experiment (CORE) protocol (Griffies et al., 2009) in which the inputs for calculating surface fluxes are taken from an atmospheric reanalysis data set adjusted so as to better agree with in-situ measurements. Sensible and latent heat fluxes are then calculated using bulk formulae. We will refer to these simulations as the CORE runs. In CORE runs, freshwater forcing is given by a combination of applied precipitation, evaporation computed using bulk fluxes, and a correction diagnosed so as to restore surface salinities in the top 10m to climatological monthly values over 60 days. Thus the fluxes forcing the CORE runs may be thought of as a "best-guess" observationally-based estimate, but omitting important feedbacks whereby the atmosphere ensures that rainfall and evaporation are consistent with each other. The restoring correction is a crude representation of these feedbacks. Without it, many models fail to maintain a robust Atlantic Meridional Overturning circulation (see section 16 of Griffies et al., 2009 for further discussion). However, the presence of such a correction damps long-period variability in salinity, with implications for biogeoechemical cycles. The resulting difficulty in simulating long-term salinity variability forms an important part of our motivation for examining coupled climate models.

The CORE models are initialized from the World Ocean Atlas database with respect to temperature, salinity, nitrate, phosphate and silicate. Seven cycles of the 46 years of observed forcing are then applied, comprising a run of 322 years. While this is insufficient to spin up the deep ocean carbon cycle, surface nutrients, biomass, and productivity come to near-equilibrium

fairly rapidly. For example, the average relative change in surface large phytoplankton concentration is less than 3% between the final two cycles and the average total biomass changes by 0-0.8% over depths ranging from 100m to the surface.

c.) Coupled climate model

In coupled climate models, the incoming solar radiation, atmospheric greenhouse gases and aerosols, and some aspects of the land surface are fixed, but the air-sea fluxes of heat and momentum are then allowed to evolve freely. In coupled climate models, the surface fluxes may deviate from the best observationally-based fluxes, but they do so in a consistent way (a cool bias will cause a decrease in evaporation which then results in decrease in precipitation). Such models can simulate the mean climate, its forced response to changes in the radiation balance and its intrinsic variability, but will not simulate the response of climate in any given year. One should thus look to the coupled models to match statistical relationships between biological features and physical forcing, not to simulate individual years or decades.

The model used for these runs is the Geophysical Fluid Dynamics Laboratory's Earth System Model 2.1 (ESM2.1). The physical core of this model is the CM2.1 global coupled climate model described in Delworth et al. (2006), with the baseline ocean solution described in Gnanadesikan et al. (2006). CM2.1 has an atmospheric physical climate that compares well against other global climate models (Reichler and Kim, 2008), an ocean circulation in the Southern Ocean that is quite realistic (Russell, Stouffer and Dixon, 2006) and a relatively realistic ENSO (Wittenberg et al., 2006; van Oldenborgh et al., 2005). The physical model is initialized from the CM2.1 1860 control run after 2000 years of run. ESM2.1 is initialized with

observed nutrients from the World Ocean Atlas and then run with interactive chlorophyll and an interactive land biosphere but with radiative gasses at 1860 levels for another 1600 years. Output is then taken from the last century of this simulation. Variability seen in the coupled model should thus reflect the background level of unforced, internal variability in the climate system.

3. Results

a.) Model evaluation

Differences between the models are summarized in Figure 1 and statistical comparison of the temperature, salinity, phosphate, nitrate and the natural log of surface chlorophyll is presented in Table 1. Zonally averaged errors in sea surface temperature (black solid line, Figure 1a) show a strong warm bias in the Southern Ocean resulting from an excess of summertime shortwave radiation, and a cold bias elsewhere. The low-latitude cold bias probably contributes to lower evaporation rates and a fresh bias (red solid line, Figure 1a) The CORE model tends to be biased cold (dashed black line, Figure 1a) and slightly salty (dashed red line, Figure 1a)- illustrating the limits of the restoring correction in actually fixing surface salinities to observations. The RMS temperature error of 1.43C is only slightly larger than the 1.28C seen in the 1990 control run of the CM2.1 coupled climate model by Gnanadesikan et al. (2006) and is essentially identical to CM2.1 without interactive biology when it is run out for 1600 years. The changes in ocean shortwave absorption and land hydrology induced by including prognostic biology do not significantly alter the previously published solution. The three-dimensional temperature and salinity fields match the data slightly better than the MPI, NCAR and IPSL models reported in Schneider et al., (2008).

The annual cycle of mixed layer depth (Figure 1b) shows that the models capture the range of mixed layer depth in mid-latitudes, but tend to have deeper mixed layers in the wintertime high latitudes (particularly in the North Atlantic and the Southern Ocean) than observed. Summertime mixed layers are close to observational values in the North Atlantic Pacific but tend to be too shallow in the Southern Ocean in both models.

Examining the profile of salinity at a number of locations (Figure 1c) we see that both models capture the contrast between the salty North Atlantic (black lines), fresh North Pacific (red lines), with the Southern Ocean lying in between the two. ESM2.1, by contrast, also predicts a distinct salinity minima at about the right depth in both locations, though the North Pacific and Southern Ocean are both too salty. Closer examination, however, shows that the CORE model (dashed lines) fails to reproduce these salinity minima seen in both the North Pacific and Southern Ocean, suggesting an overly weak formation of mode and intermediate waters, but a flushing of the deep ocean with cold, fresh bottom water- consistent with overly high mixed layer depths in the Southern Ocean.

This stronger circulation of Antarctic Bottom Water is reflected in the overturning streamfunction at 30S (blue lines, Figure 1d), which is extremely weak in ESM2.1 (as it is in all of the CM2.1 series) but reaches 11.2 Sv of AABW export in the CORE runs, about 4.3 Sv occurs in the Atlantic basin. However, this circulation fails to upwell in the North Pacific in either the CORE or ESM2.1 simulations (red lines, Fig. 1d), though the ESM2.1 model does show an overturning cell above 1000m consistent with the formation of the North Pacific Intermediate Water salinity minimum. Both models show a significant North Atlantic overturning, with ESM2.1 predicting a somewhat deeper maximum of 23.5 Sv, while the CORE simulation gives 16.9 Sv.

The best characterized biogeochemical fields with which the models can be compared are the spatial distribution of macronutrients. As shown by the thick black dashed line in Figure 2a, the CORE ocean-ice model captures the large-scale distribution of surface phosphate and nitrate, with higher values along the equator, higher values in the northern subpolar gyres and the highest values in the Southern Ocean. The model also captures the tendency towards nitrate limitation that allows for unutilized phosphate in the subtropical gyres, where nitrate essentially goes to zero (red lines). Correlations with observed surface nutrients exceed 0.95. The main error visible in Figure 2a is the underestimate of surface phosphate in the northern oceans, which is notably worse in ESM2.1 than in CM2.1. Profiles of nutrients in the North Pacific (red lines, Figure 2b) show that the phosphate deficit penetrates to much greater depths, possibly reflecting the lack of deep upwelling seen in Figure 1d. The CORE model has a much reduced bias in phosphate concentration in the North Pacific possibly because of the lack of deep upwelling is balanced by a lack of lateral export (reflected in the lack of 1000m salinity minimum in Figure 1c) and possibly because it has only been run out for 1/5 the time as ESM2.1. The three-dimensional correlation of phosphate with observations in ESM2.1 (0.84) is comparable to the 0.82-0.86 reported Schneider et al. (2008) for the NCAR, MPIM and IPSL models. The three-dimensional correlation with nitrate is lower and nitrate is biased low in the global, largely because the oxygen minimum zones become too intense in this model, resulting in overly intense dentrification. As surface nutrients are relatively realistic, however, we suspect that the overly high rates of denitrification are being compensated by excessive nitrogen fixation.

Additional constraints on the model can be gleaned by comparing with products inferred from satellite remote sensing. The zonal integral of chlorophyll (Figure 2c), which is very similar between the ocean-only and coupled models, tends to underestimate the total chlorophyll

inventory in part due to a failure to capture very high values in upwelling zones. The chlorophyll signal shows that low simulated surface nutrients in high northern latitudes are not due to an excess of productivity, suggesting that insufficient nutrient supply may be responsible. Both the CORE and ESM2.1 simulations capture about half the observed spatial variance in the log of annually averaged chlorophyll with an underestimate of about 8% globally (Table 1). Zonal-mean primary productivity is essentially identical with that estimated from SeaWiFS chlorophyll using the Carr, (2002) algorithm, (Figure 2d) in both the ocean-only and coupled models, though given that the differences between the models and observational estimates is considerably smaller than differences between individual observational estimates (Gnanadesikan et al., 2004) and less than the uncertainty in chlorophyll retrievals the agreement may be fortuitous.

c.) Size structure and the disproportionate variability of large phytoplankton

We begin by examining the relative interannual variability of a number of fields, using the coefficient of variation (standard deviation/mean) of the annually smoothed field as a metric. For the first seven years of the SeaWiFS mission, the coefficient of variation of chlorophyll (Fig. 3a) and productivity (Fig.3b) is less than 0.1 over most of the global ocean. Assuming purely sinusoidal variation, a coefficient of variation of 0.1 would imply variation from 0.86 to 1.14 times the mean value. The largest relative variability is seen not in the center of the high-chlorophyll equatorial upwelling or subpolar gyres, but instead along the edges. A similar picture was seen by Martinez et al. (2009) when looking at interdecadal variability of chlorophyll when comparing the SeaWiFS and CZCS satellite products. Comparing the short SeaWiFS time series with the last 46-year cycle of the CORE-forced runs, we see a similar concentration of

interannual variability along the edges of the equatorial cold tongue and at the edges of the subtropical gyres. The coefficient of variation for modeled productivity is generally smaller than for modeled chlorophyll, though the spatial patterns of the log of the variation are correlated with a coefficient of 0.76. As shown by the regression coefficient in the lower right of Figure 3d, a 10% change in model chlorophyll would only be expected to produce a 5.2% change in productivity. A powerlaw dependence is found in algorithms for computing primary productivity from satellite-estimated chlorophyll (compare Fig. 3a,b), as higher chlorophyll leads to higher light-harvesting capacity but also less penetration of solar radiation.

As might be expected from (6), the models predict very different variability for the biomass of large and small phytoplankton. Over most of the ocean, the coefficient of variation of small phytoplankton biomass (Fig 3e) is less than 10%, much smaller than for total chlorophyll. The pattern of chlorophyll variability is correlated with the changes in small biomass, with a correlation coefficient of 0.58 in the CORE run. However, a 10% change in chlorophyll only results in a 1.8% change in small plankton biomass. By contrast, the coefficient of variation for large plankton biomass (Figure 3f) is comparable to (and along the equatorial cold tongue much larger than) the coefficient of variation of chlorophyll. The bulk of the variability in productivity is thus in the large phytoplankton, not the small- even though small plankton make up the majority of the global phytoplankton biomass. The coupled model (not shown), shows similar patterns of variability as the CORE-forced simulation with much more variability in large phytoplankton, similar correlation and regression coefficients between chlorophyll and other fields, and the largest-amplitude variability occurring at the edge of the subtropical gyres and coastal upwelling regions.

Comparing the zonal average of the coefficient of variation of large phytoplankton biomass on interannual time scales (Figure 4a) further emphasizes the difference between small and large phytoplankton. The standard deviation of the total biomass (solid lines) is on average less than 10% of the mean over almost the entire ocean in both the ocean-only and coupled models. By constrast, for large biomass over the tropics a relative standard deviation of 35% is seen in both models. Interannual variability in the diatom biomass (blue lines, Figure 4) largely tracks that of large phytoplankton biomass in the CORE runs (this variable was not saved for the ESM2.1 runs).

Variability in the annual productivity is not, however, the only possible way in which biogeochemical variability can project into interannual changes in ecosystems. The "match-mismatch" hypothesis of Cushing (1990) builds on the classic work of Hjort (1914), suggesting that changes in the timing of spring bloom are more important than changes in the magnitude of productivity. Analyzing interannual variability in productivity month by month, with a particular focus on the spring bloom, we find that the models predict more variability in the spring season. During April, the coefficients of variation of total plankton biomass, diatom biomass, and large plankton biomass all increase increase in high northern latitudes. The largest change is seen for large plankton biomass between 60N and 80N (dashed lines), where the coefficient of variation increases from 0.10-0.12 in the annual mean to the ~0.5 during April in the CORE model and 0.75-0.80 during April in ESM2.1. By contrast, the coefficient of variation goes from about 0.3 in the annual mean to about 0.4 for April alone for large phytoplankton in the tropics, a much smaller increase. Relative variability remains relatively small throughout the Southern Hemisphere. Roughly the opposite geographic pattern is seen in the austral spring (October, Figure 4d), with the Southern Hemisphere showing a large increase south of 60S, with the

average coefficient of varation of large biomass reaching 0.7 at some latitudes. Again we see that the CORE forced model tends to have less variability than ESM2.1 at high latitudes and a little more variability in the tropics. The month of July (Figure 4c) looks more like the interannual variability, with a tropical peak and lower values in the high latitudes. The actual values are higher, as the mean coefficient from 30S to 30N is 0.35 in ESM2.1 during July vs. 0.24 in the annually-smoothed version, but this is a much smaller increase than that seen at high latitudes. As discussed below, changes in when productivity occurs during the year are most important at high latitudes, whereas in low latitudes interannual changes in the annual mean productivity are much more important.

As shown in Figure 5, the basic spatial pattern of interannual variability in the springtime large phytoplankton biomass in ESM2.1 resembles that seen in the chlorophyll, but with a much greater range. As in the SeaWiFS annual data, regions of high variability are seen at the boundary between the subtropical gyre and the high-nutrient equatorial zone, but also in mode water formation regions where deep mixed layers are found along the boundary of the subtropical and subpolar gyres. High variability is also found in convective regions within the subpolar Weddell Sea, Bering Sea, and North Atlantic. The difference between the left and right-hand columns of Figure 5 reinforces the result from Figures 3 and 4 that chlorophyll or total biomass alone can give an inaccurate picture of the interannual variability within an ecosystem.

The three key results of this section are thus that large plankton and diatoms vary more than small plankton, that large relatively variability is found on the edges of highly productive regions, and that relative variability during the spring bloom is larger than variability over the entire year. The following section expands upon the second of these results, looking at the

boundary between the equatorial upwelling and subtropical gyre, showing that the changes in concentration are associated with changes in the areal extent of the oligotrophic gyre, and considering the physical forcing driving such changes. Section 5 examines mechanisms behind springtime variation in large phytoplankton concentrations in four regions: the subtropical gyre off Hawaii, the Kuroshio extension, the Sea of Okhotsk and the Western Bering Sea. As interannual variability in diatoms largely tracks these variations in the CORE-forced runs in these regions, we expect the results to be qualitatively applicable to diatoms as well.

4. Interannual changes in biome area: The case of the equatorial upwelling

We begin with the equatorial Pacific where interannual variability is high and breaking down this variation month by month yields less of an increase (Fig. 3) than in high latitudes. The variability in this region is relatively consistent between the CORE and ESM2.1 runs, with both models simulating the largest variability around the edge of the high-nutrient cold tongue- a picture similar to that seen in Figure 3a and with the work of Martinez et al. (2009). If we define the boundary between the equatorial upwelling biome and oligotrophic gyre/subtropical biome either by using the chl=0.07 mg/m^3 isoline (following Polovina et al., 2008) or the NO_3=0.02 mmol/m^3 line (Figure 6a) between 20S and 20N, we see that the CORE model shows the gyres expanding and contracting with decadal and interannual frequencies. Although nitrate is only one of the sources of nitrogen for the off-equatorial regions in this model, it is used as an indicator of upwelled nutrient. The changes in oligotrophic gyre area can be regressed onto changes in chlorophyll (colors, Fig. 6b) showing that a larger oligotrophic gyre area is associated with lower chlorophyll concentrations at the edge of the high nutrient waters. Regressing gyre area onto

wind stresses (vectors, Figure 6b), shows that higher oligotrophic gyre areas are associated with anomalous easterlies along the gyre margins. The correlation between equatorial winds and tropical oligotrophic gyre area over this time period is 0.77, while off-equator, the correlations approach 0.85.

We examine the mechanistic connection between winds, currents and the area of the subtropical biome by looking at the mass balance of nitrogen in the CORE runs in three areas outlined by the green lines in Figure 7b. Changes in nitrate import that explain a large fraction of changes in the vertical particle export flux can be identified as important causative agents for export flux variability. Which fluxes are the most important end up being slightly different for the regions on and off the equator. Along the equator (175E-160W, 3S-3N) the anomalous advection of nitrate from below and from the east together (red line, Fig. 7a) correlate well with the particle export anomaly at 100m (black line Fig. 7a). However, this correlation is not simply due to the direct response of wind-driven currents acting on the background nutrient field. The flux due to changes in currents alone (blue line, Fig. 7a) has a strikingly lower correlation with the particle export (0.36 vs. 0.9) and a lower amplitude of variability. In the northern center of action (165W-140W, 5N-15N) the dominant control of the particle export is from advection of nutrient into the region from the south (compare black and red lines, Fig. 7b). Here too, however, changes in the velocity alone account for only a small part of the variability, implying that changes in the nutrient concentrations of the inflow are dominant. The dominance both of north-south advection and of changes in nutrient concentrations in explaining such changes in advective flux is also found in the region from 140W-100W, 8S-15S (Figure 7c). This region covers the southern center of action in Figure 6b (while the blue and black lines do not in fact look well correlated, they in fact match up extremely well until the 1980s). In all three regions,

the changes in export represent changes in the regional extent of the highly productive, nutrient rich waters, not just local changes in productivity. This implies that predicting the change in biome area involves more than just predicting changes in the amplitude of ENSO- one must also understand the changes in the background field of nutrients.

5. Variability of large phytoplankton biomass in the North Pacific during boreal spring

a.) Identification of different regimes

Turning to variability associated with the spring bloom, we see that the relationship between local sea surface temperature and biological cycling during April shows a complicated pattern in the North Pacific (Figure 8a and b). The correlation patterns of chlorophyll and large plankton biomass and SST show a rough consistency, with a tongue of high variability negatively correlated with SST extending from the center of the subtropical gyre to the northeast off the Pacific coast of Canada, weak positive correlation in the northwest Pacific, stronger positive correlation Sea of Okhotsk and a region of strong negative correlation in the western Bering Sea off of Kamchatka. However, the coefficients of variation of chlorophyll and large phytoplankton biomass are only of similar magnitude in the first of these regions. In the region from 150E-160E and 36N-40N (in the Kuroshio extension) the coefficient of variation of chlorophyll is 0.35 as opposed to 0.98 for large phytoplankton biomass and similar differences are found in the Sea of Okhotsk and Western Bering Sea. In all four regions (but particularly the ones outside the subtropical gyre), the coefficient of variation of large biomass during April is larger than either March, May or the entire time period from March to May. In the Kuroshio extension, for example, the coefficient of variation for large phytoplankton biomass during the

entire March-April-May time period is only 0.24, about ¼ that of the April time period alone. Such differences are consistent with the interannual variability in April biomass being primarily driven by variability in bloom timing rather reflecting interannual changes in the magnitude of seasonal productivity. As shown in the following sections, the physical mechanisms underlying this variability differ in each of the regimes denoted by the green boxes in Figure 8.

The drivers of variation in large phytoplankton biomass during the month of April are analysed by correlating this variability with SST, SSS, the salinity difference between the surface and 150m, wind speed, the natural log of the mixed layer depth, nitrate and dissolved iron concentrations (Figure 9) for each of the boxes in Figure 8. Correlations with April conditions (right-hand set of bars in each panel in Figure 9) are shown to isolate the mechanisms driving the interannual changes in biomass, while correlations with January conditions (left-hand set of bars in each panel) are shown to isolate whether the environmental controls are potentially predictable from oceanic conditions earlier in the year.

b.) The subtropical gyre

In the subtropical gyres, downwelling and high vertical gradients in temperature combine to create regions with low surface nutrients. Although sometimes referred to as biological deserts, these regions do support some pelagic fisheries. In such nutrient-limited low-latitude regimes one would expect surface cooling to lead to more mixing, more nutrient supply and thus higher productivity. Thus mixed layer depth would be expected to be positively correlated with biomass and chlorophyll in tropical and subtropical regions. Follows and Dutkewicz (2002) compared a model forced in a similar manner to ours with SeaWiFS chlorophyll in the subtropics.

Comparing modeled mixed layer depth and observed chlorophyll, their work supported the idea that the increased chlorophyll was associated with increased vertical supply of nutrients.

. Examining the subtropical North Pacific near Hawaii, from 170W-160W and 26-30N we see a basic consistency with the classic picture (Figure 9a). During the month of April, high phytoplankton biomass is best correlated with high levels of nitrate and anticorrelated with sea surface temperature. However, it does not appear to be the case that deep mixed layers during April are necessary for high biomass during the same month. Instead high phytoplankton biomass during April is (weakly) associated with *shallower* mixed layers, higher light and weaker winds. A correlation between April biomass and deeper mixed layers (associated with higher winds and cooler SSTs) only appears the when the previous January is considered. That the correlation between April large biomass and January mixed layer depth is smaller in magnitude than the anticorrelation with temperature also suggests that some of the variability in nutrient may result from southward advection of colder, fresher northern waters and not just to deeper local mixing. The negative correlation with iron shows that iron cannot be the dominant limiting nutrient but is instead drawn down more by high levels of biological activity. Because we model nutrient limitation using Liebig's law of the minimum (eqns 1 and 4), iron limitation in this version of our model only has an impact is when it is less limiting that nitrogen, which only occurs in the Southern Ocean, in the Peru upwelling and the Pacific cold tongue.

c.) The Kuroshio extension- a mode water formation region

Moving further to the north, we come to a region that has a strong seasonal cycle in mixed layer depth at the edge of the subtropical gyre. Deeper wintertime mixing means that

springtime light limitation can be more extreme in this region, which is associated with formation of key mode waters. Nutrients in the Kuroshio extension are more abundant than in the subtropical gyre, though at lower levels than in the subpolar gyre, with the result that chlorophyll levels are somewhat lower than in the subpolar gyre. Sarmiento et al. (2004) defined this region as a combination between the subtropical seasonal stratified biome and subpolar gyre biome, while Polovina et al. (this volume) include it in the temperate biome. As shown in Figures 8b and 9b, the large interannual variability in April large phytoplankton biomass in this region is only weakly correlated with temperature, but is very strongly *anticorrelated* with mixed layer depth and positively correlated with mixed layer light availability. Light limitation, rather than nutrient limitation plays a dominant role here so that the springtime shallowing of the mixed layer triggers a bloom. Note that there is no nutrient limitation during April despite the annual-mean nutrient concentrations being somewhat low in this area (Figure 2a)- so that such (unrealistic) limitation kicks in later during the summer. Shallow mixed layers can result from low winds (hence the anticorrelation with wind). They can also either be associated local warming, or from the advection of fresher, colder waters from the north, hence the weak correlation with sea surface temperature. In contrast to the center of the subtropical gyre, there is relatively little correlation with conditions in January, suggesting that this will be a challenging region to predict.

d.) The Sea of Okhotsk- A marginal ice zone biome

A third region outlined in Figure 8 is the Sea of Okhotsk, which is ice covered during the wintertime and as such was classified by Sarmiento et al. (2004) as part of the marginal ice zone biome. Interannual variability of large phytoplankton biomass in this region is strongly correlated with temperature and light availability, but only weakly anticorrelated with mixed layer depth (Figure 9c). The correlation between April large phytoplankton biomass and sea ice concentration (not shown) is -0.72, comparable to the 0.86 correlation with mixed layer light. This is consistent with variability in the timing of ice breakup being important for allowing relief of light limitation and drawdown of surface nutrient, and also with higher SSTs being associated with this breakup.

The correlation between mixed layer light and chlorophyll in this region (0.50, not shown) is much lower than the correlation between mixed layer light and both large and small phytoplankton biomass (0.86). This reflects the fact, previously noted, that the phytoplankton in the TOPAZ model adapt to light availability, reducing their chlorophyll to carbon ratio as more light becomes available (equation 4). As a result, the chlorophyll to carbon ratio in the Sea of Okhotsk during the month of April is strongly anticorrelated with mixed layer light (-0.63) reducing the amplitude of chlorophyll variability and showing again why it is necessary to be cautious in extrapolating from satellite chlorophyll to ecosystem state.

e.) The Western Bering Sea- A salinity stratified subpolar biome

A final region of interest is found in the western Bering Sea, where there is large interannual variability in large phytoplankton biomass but an anticorrelation with temperature. As shown in Figure 9d, this region is also light limited, and large phytoplankton biomass is

strongly anticorrelated with mixed layer depth. The anticorrelation with temperature (implying that cold temperatures are correlated with shallow mixed layers) stands in contrast to the Kuroshio extension and Sea of Okhotsk and means that salinity rather than temperature is the dominant mechanism establishing mixed layer stratification in this region. This dynamical regime is also found in many other parts of the model ocean, including the southern Labrador Sea, central Norwegian Sea and Weddell Sea.

The mechanisms by which such salinity anomalies develop are potentially complicated. Gargett (1997) looked at salmon stocks in the North Pacific and argued that the key variable for explaining coastal stability was Alaskan streamflow, which freshened coastal regions and was tied to the changes in low pressure associated with the PDO. However other analysis we have done of the CM2.1 model (Gnanadesikan et al., Variability of ventilation in the North Pacific in a coupled model, in prep.) in our modelled western Bering Sea suggests that the dominant driver of salinity variability is not the supply of fresh water, but rather the upwelling of salty deep water from below as a result of local changes in the wind stress curl. Galbraith et al. (subm.) look at similar salinity anomalies in a coarse-resolution coupled model in the Southern Ocean, and find that the source of the anomalies is a combination of precipitation anomalies and entrainment of saltier deep waters.

6. Discussion and conclusions

The coupled physical-biogeochemical models used to assess climate change impacts on ocean ecosystem offer insights as to how changing prey availability for fisheries may be linked to

climate. We review these insights below, and consider the potential implications for predicting and diagnosing marine ecosystem variability.

a.) The importance of size structure

The first major message of this paper is that one should not expect a straightforward scaling between primary productivity or chlorophyll and the biomass of the large phytoplankton that are thought to be most important for fisheries. Over much of the ocean, large plankton appear to respond disproportionately to changes in environmental conditions, driven by differential uptake of nutrients and a size-dependent grazing parameterization (Fig 2d, 3-5,8). Because photoadaptation causes the chl:C ratio to drop as more light becomes available, regions which are light limited show much less variability in chlorophyll than in large plankton biomass. This suggests that in order to track prey availability, fisheries oceanographers need to look to satellite estimates of phytoplankton carbon biomass (such as that proposed by Behrenfeld et al. 2005) as well as those that separate out phytoplankton into different size classes (Kostadinov et al., 2009, Mouw et al. , subm). Algorithms for isolating the diatom component (for example Alvain et al., 2008) may be important as well. Although diatoms are well correlated with large phytoplankton biomass in one of our runs, there are some differences in detail in terms of the location of maximum variability, and our parameterization of diatom fraction is crude. Although these products remain preliminary, the fisheries oceanography community should consider using them, especially where results from chlorophyll or primary productivity seem to contradict inferences made from looking at fisheries data. Additionally, when examining simulations from earth system models, fisheries oceanographers should request size structured

biomass, which is often simulated by such models, and not be content with modeled chlorophyll or primary productivity.

b.) The potential importance of timing

The second key message of this paper is that models show much more variation in the interannual variability of phytoplankton biomass associated with the spring bloom than in the interannual variability in annually averaged phytoplankton biomass. For high latitude regions and also when large phytoplankton are considered in isolation the difference can approach an order of magnitude-supporting the Hjort-Cushing "match-mismatch" hypothesis. Larger variability in bloom timing relative to interannually integrated production has been seen in individual ecosystems (e.g. Henson and Thomas, 2005; Hunt et al., 2008), but this study breaks new ground in looking at the global distribution of the coefficient of variation of large phytoplankton biomass during the spring. Variability in bloom timing has potentially important implications for fisheries oceanographers using models such as Ecopath, which often either use annual integrated primary productivity (Guennette et al., 2006; Howell et al., 2010) or diagnose this quantity from lower trophic level biomass (Piroddi et al., 2010). Our results suggest that such models may need to take bloom timing into account if they are to properly estimate the range of climate-forced ecosystem variability.

Bloom timing may be particularly important for understanding different climate reponses between "capital breeders" which build up a large stock of resources before breeding, and "income breeders" which match food and breeding (Jonsson, 1997). For example, Boulcott and Wright (2008) argue that variability in the timing of blooms in the North Sea has a particularly

strong impact on the regional distribution of sandeels. Insofar as income breeders average over the entire seasonal cycle, by contrast, they may be less vulnerable to such variability, as noted by Martin and Wiebe (2004) for arctic and alpine birds and Takasuka et al. (2010) for Japanese anchovy as opposed to Japanese sardine. Understanding such tradeoffs may be a fruitful area of collaboration between biogeochemical modelers and fisheries oceanographers.

c.) Changes in tropical biome extent: implications for predictability

Both observations and models (Figs 3, 5) show the large relative variability on the edges rather than in the centers of highly productive regions. This may be important, as many organisms have planktonic larval stages, and many of the highly productive regions (in particular coastal and equatorial upwelling zones) are divergent. Larvae spawned in such regions may thus be carried out of them on time scales of a few weeks, and whether they are able to return may depend more on the food they find on the edges of the unproductive gyres than in the center of the upwelling regions. We suggest more study of whether larval survival within these edge regions is important for certain species. Additionally, the edges of high productivity regions may be more favorable for visual predators such as tuna, which may trade off the requirement for relatively clear water in order to detect and capture prey with higher prey densities in more turbid waters (Kirby et al., 2000).

Variations in the edges of the gyres have been linked to climate change by Polovina et al. (2008) who saw an increase in the area of the oligotrophic gyres during the SeaWiFS era. However, when Henson et al. (2010) compared historical trends in gyre area with several CORE-forced ocean biogeochemistry models (including the one used here) they found a generally good

agreement between modeled and observed gyre size (0.88 for the SeaWiFS era) but also found that the variability during the SeaWiFS era was much smaller than that required to detect an anthropogenic signal. Given the deficiencies of an Eulerian interpretation of ocean biome variability on short time scales (Figure 7) as well as previous results indicating that there are changes in the large-scale ventilation structure of the ocean under global warming (Gnanadesikan et al., 2007), it will be essential not to depend on physical models alone to predict the behavior of these biome boundaries.

d.) Challenges in modeling high latitude variability

We have shown that interannual variation in the monthly distribution of productivity may be much larger than the interannual variation in the mean productivity (Fig. 4,5) and that in high latitudes salinity can play an important role in explaining this variability (Fig. 9). Variability in salinity presents a challenge to retrospective analyses of ecosystem variability. As seen in Figures 4 and 5 the high latitude variation in springtime production is higher in ESM2.1 coupled climate models than in the CORE ocean-only reanalysis model. The main reason for this is that ocean-only models run with "observed" precipitation must be also run with a flux correction by which salinities are restored to their climatological values. Without such a restoring, a chain of feedbacks may be triggered at high latitudes whereby cooling in convective regions leads to precipitation exceeding evaporation, resulting in a buildup of freshwater at the surface, suppression of convection, and further cooling. In the real world, cooling a drop in surface temperatures would also be expected to lead to a decrease in precipitation, but this feedback is absent in CORE-forced runs. However the presence of restoring can damp interannual variability

in salinity, especially when it is associated with large-scale advection of surface anomalies. The challenge then is for the climate community to develop methods of reanalysis that can properly simulate the variability in winds and heating without damping out hydrological feedbacks. Coupled reanalyses (Zhang et al., 2007) in which the atmospheric winds are nudged towards observed values may provide such consistent solution, but ecosystem models have yet to be included in these systems. In the interim, fisheries oceanographers using CORE-forced runs need to carefully evaluate whether observed salinity variability is properly captured.

Acknowledgments: Rob Armstrong and Jorge Sarmiento helped formulate our original implementation of size structure within the models. Charlie Stock, Ryan Rykaczewski and Vince Saba have helped us understand the implications and limitations of this approach and provided useful reviews of this manuscript. Thanks to Jon Hare for useful discussions and for the invitation to give this talk at the Sendai Meeting and to Shin-Ichi Ito and two anonymous reviewers for their comments on a previous version on this manuscript.

References

Agawin, N. S. R., Duarte, C.M, and Agusti,S. 2000. Nutrient and temperature control of the contribution of picoplankton to phytoplankton biomass and production, Limnology and Oceanogrraphy, 45: 591– 600.

Aita, M.N., Yamanaka, Y., and M. J. Kishi, M.J. 2003. Effect of ontogenetic vertical migration of zooplankton on the results of NEMURO embedded in a general circulation model. Fisheries Oceanography, 12, 284-290

Aita, M. N., Yamanaka, Y. and Kishi, M.J. 2007. Interdecadal variation of the lower trophic ecosystem in the Northern Pacific between 1948 and 2002, in a 3-D implementation of the NEMURO model. Ecological Modelling, 202, 81-91.

Alvain, S., Moulin, C., Dandonneau, Y., and Loisel, H., 2008. Seasonal distribution and succession 10 of dominant phytoplankton groups in the global ocean: A satellite view, *Global Biogeochem. Cy.*, 22, GB3001, doi:10.1029/2007GB003154.

Aumont, O., and Bopp, L. 2006. Globalizing results from ocean in situ iron fertilization studies: Global Biogeochemical Cycles, 20: GB2017 doi:10.1029/2005GB002591.

Behrenfeld, M.J., Boss, E., Siegel, D.A. and Shea, D.M. 2005. Carbon-based ocean productivity and phytoplankton physiology from space, Global Biogeochemical Cycles, 19, GB1006, doi:10.1029/2004GB002299.

Bigelow, H.B. 1926. Plankton of the offshore waters of the Gulf of Maine, Bulletin US Bureau of Fisheries, 40, 509pp.

Boulcott, P and Wright. P.J. 2008. Critical timing for reproductive allocation in a capital breeder: evidence from sandeels, Aquatic Biology, 3, 31-40.

Carr, M.-E. 2002. Estimation of potential productivity in Eastern Boundary Currents using remote sensing, Deep Sea Research, Part II, 49: 59–80.

Chavez, F.P., Ryan, J., Lluch-Costa, S.E. and Niquen M. 2003. From anchovies to sardines and back, multidecadal change in the Pacific Ocean, Science, 299, 217-221.

Cushing, D.H. 1990. Plankton production and year-class strength in fish populations: an update of the Match/Mismatch hypothesis, Advances in Marine Biology, 26, 249-293.

Delworth, T.L. and co-authors 2006. GFDL's CM2 global coupled climate models: Part 1-Formulation and simulation characteristics, Journal of Climate, 19: 643-674.

Dugdale, R.C. and Goering, J.J. 1967. Uptake of new and regenerated forms of nitrogen in primary productivity, Limnology and Oceanography, 12: 196-206.

Dunne, J.P., Armstrong, R.A., Gnanadesikan,A. and Sarmiento, J.L. 2005. Empirical and mechanistic models of the particle export ratio, Global Biogeochemical Cycles, 19: GB4026, doi:10.1029/2004GB002390.

Dunne, J. P., Sarmiento, J.L., and Gnanadesikan,A. 2007. A synthesis of global particle export from the surface ocean and cycling through the ocean interior and on the seafloor. Global Biogeochemical Cycles, 21: GB4006, doi:10.1029/2006GB002907.

Dunne, J.P., Galbraith, E.D., Gnanadesikan,A., John, J., Sarmiento, J.L., Slater, R.D., and Griffies, S.M. 2010. Implications of elemental coupling in a global ocean biogeochemistry/general circulation model, in prep. for Biogeosciences

Follows, M. and Dutkewicz, S. 2002. Meteorological modulation of the North Atlantic Spring Bloom, Deep Sea Research Part II, 49: 321-344.

Galbraith, E.D., Gnanadesikan, A., Dunne, J.P. and Hiscock, M.R. 2010. Regional impacts of iron-light co-limitation in a global biogeochemical model, Biogeosciences, 7: 1043-1064.

Gargett, A.E. 1997. The optimal stability "window": a mechanism underlying decadal fluctuations in North Pacific salmon stocks? Fisheries Oceanography, 5, 109-117.

Genner, M.J., Sims, D.W., Wearmouth, V.J., Southall, E.J., Southward, A.J., Henderson, P.A. and Hawkins, S.J. 2004, Regional climatic warming drives long-term community changes of British marine fish, Proceedings of the Royal Society B, 655-661.

Glynn, P.W. and deWeerdt, W.H. 1991.Elimination of two reef-building hydrocorals following the 1982-1983 El Nino warming event, Science, 253, 69-71.

Gnanadesikan A., and co-authors, 2006. GFDL's CM2 Global Coupled Climate Models- Part 2: The baseline ocean simulation, Journal of Climate, 19, 675-697.

Gnanadesikan, A., Russell, J.L. and Zeng, F. 2007. How does ocean ventilation change under global warming? Ocean Science,3, 43-53.

Griffies, S.M. and co-authors, 2009. Coordinated Ocean-ice Reference Experiments (COREs), Ocean Modelling, 26: 1-46.

Griffies, S.M. Gnanadesikan, A., Dixon, K.W., Dunne, J.P., Gerdes, R.. Harrison, M.J., Rosati, A., Russell, J. L., Samuels, B. L., Spelman, M.J., Winton, M. and Zhang, R. 2005. Formulation of an ocean model for global climate simulations. Ocean Science, 1: 45-79.

Guenette, S., Heymans, S.J.J., Christensen, V. and Trites, A.W., Ecosystem models show combined effects of fishing, predation, competition and ocean productivity on Steller sea lions, (Eumetopas jubatus) in Alaska, Canadian Journal of Fisheries and Aquatic Sciences, 63, 2495-2517, 2006.

Henson, S.A., Sarmiento, J.L., Dunne, J.P, Bopp, L., Lima, I., Doney, S.C., John, J. and Beaulieu, C. 2010. Detection of anthropogenic climate change in satellite records of ocean chlorophyll and productivity, Biogeosciences, 7, 621-640.

Henson, S. and Thomas, A. 2007. Interannnual variability in timing of bloom initiation in the California Current System, Journal of Geophysical Research Oceans, 112, C08007, doi:10.1029/2006JC003960.

Hjort, J. 1914. Fluctuations in the great fisheries of northern Europe viewed in the light of biological research. Rapp. Cons. Explor. Mer., 20:1-228.

Howell, E.A., Dunne, J.P. and Polovina, J.J. 2010. Modelling the central North Pacific ecosystem response to predicted climate variations and fishery management scenarios, Climate Change Effects on Fish and Fisheries, Sendai, Japan, 139.

Hunt, G.L., Stabeno, P., Walters, G., Sinclair, E., Brodeur, R., Napp, J.M. and Bond, N.A., 2002. Climate change and control of the southeastern Bering Sea pelagic ecosystem, Deep Sea Res. II, 49, 5821-5853.

Jonsson, K.I. 1997. Capital and income breeding as alternative tactics of resource use in reproduction, Oikos, 78, 57-66.

Kishi,M.J., Kaeriyama,M., Ueno, H. and Kamezawa, Y. 2010. The effect of climate change on the growth of Japanese chum salmon (Oncorhynchus keta) using a bioenergetics model coupled with a three-dimensional lower tropic ecosystem model (NEMURO). Deep-Sea Research II 57, 1257–1265

Kimura, S. and Tsukamoto, K., 2006. The salinity front in the North Equatorial Current: A landmark for the spawning migration of the Japanese eel (Anguilla japonica) related to the stock recruitment. Deep-Sea Research II, 53, 315-325.

Klausmeier, C., E. Litchman, Daufresne, T. and Levin, S.A., 2004. Optimal nitrogen-to-phosphorus stoichiometry of phytoplankton, Nature, 429, 171-174.

Kirby, D.S., Fiksen, O., Hart, D.J.B. 2000. A dynamic optimisation model for the behaviour of tunas at ocean fronts, Fisheries Oceanography, 9, 328-342.

Kostadinov, T.S., Siegel, D.A., and Maritorena, S. 2009. Retrieval of the particle size distribution from satellite ocean color observations. Journal of Geophysical Research – Oceans, 114: C09015, doi:10.1029/2009JC005303.

Mantua, N.R., Hare, S.R., Zhang, Y., Wallace, J.M. and Francis, R.C. 1997. A Pacific interdecadal climate oscillation with impacts on salmon production, Bulletin of the American Meteorological Society, 78: 1069-1079.

Martin, K. and Wiebe, K.L. 2004. Coping mechanisms of alpine and arctic breeding birds: Extreme weather and limitations to reproductive resilience, Integrative and Comparative Biology, 44, 177-185.

Martinez, E., Antoine, D., D'Ortenzio, F. and Gentili, B. 2009. Climate-driven basin-scale decadal oscillations of oceanic phytoplankton, Science: 326, 1253-1256.

Moore, J.K., Doney, S.C., Kleypas, J.A., Glover, D.M., and Fung, I.Y. 2002. An intermediate complexity marine ecosystem model for the global domain: Deep-Sea Research II, 49: 463-507.

Platt, T., Subba Rao, D.V. and Irwin, B., 1983. Photosynthesis of picoplankton in the oligotrophic ocean, Nature, 301, 702-704.

Polovina, J.J., Howell, E.A. and Abecassis, M. 2008. Ocean's least productive waters are expanding, Geophysical Research Letters, 35, L03618, doi:10.1029/2007GL031745.

Reichler, T. and Kim, J. 2008. How well do coupled climate models simulate today's climate?, Bulletin of the American Meteorological Society, 89: 303–311.

Russell, J.L., Stouffer, R.J. and Dixon, K.W. 2006. Intercomparison of the Southern Ocean Circulations in IPCC Coupled Model Control Simulations. Journal of Climate, 19(18): 4560-4575, doi:10.1175/JCLI3869.1.

Ryther, J.H. 1969. Photosynthesis and fish production in the sea, Science, 166, 72-76.

Schneider, B., Bopp, L., Gehlen, M., Segschneider, J., Frolicher, T.L., Cadule, P., Friedlingstein, P., Doney, S.C., Behrenfeld, M.J. and Joos, F. 2008. Climate-induced interannual variability of marine primary and export production in three global coupled carbon cycle models, Biogeosciences, 5, 597-614, doi:10.5194/bg-597-2008.

Six, K.D. and Meier-Reimer E. 1996. Effects of plankton dynamics on seasonal carbon fluxes in an ocean general circulation model, Global Biogeochemical Cycles, 10, 559-583.

Steinacher, M., Joos, F., Frohlicher, T, and coauthors 2010. Projected 21st century decrease in marine productivity: a multi-model analysis, Biogeosciences, 7, 979-1005, doi:10.5194/bg-7-979-2010.

Sugimoto, T., Kimura, S. and Tadokoro, K. 2001. Impact of El Nino events and climate regime shift on living resources in the western North Pacific, Progress in Oceanography, 49, 113-127.

Takasuka, A., McClatchie, S., Weber, E., Oozeki, Y., Kameda, T., Hirota, Y. and Okamura, H. 2010. Responses of anchovy and sardine spawning to physical and biological factors in the Kuroshio and California Current systems: Interspecific and intersystem comparison, in Climate Change Effects on Fish and Fisheries, Sendai Japan, 107.

Uitz, J., Claustre, H., Gentili, B. and Stramski, D. 2010: Phytoplankton class-specific primary production in the world's oceans: Seasonal and interannual variability from satellite observations, Global Biogeochemical Cycles, 24, GB3016, 10.1029/2009GB003680.

van Oldenborgh, G. J., Philip, S. Y., and Collins, M. 2005. El Nino in a changing climate: a multi-model study, Ocean Science, 1: 81–95.

Wittenberg, A. T., Rosati, A., Lau, N. G., and Ploshay, J. J. 2006. GFDL's CM2 Global coupled climate models, Part III: Tropical Pacific Climate and ENSO, J. Climate, 19, 698–722.

Zhang, S., Harrison, M.J., Rosati, A. and Wittenberg, A.T., 2007. System System Design and Evaluation of Coupled Ensemble Data Assimilation for Global Oceanic Climate Studies. Monthly Weather Review, 135(10), 3541-3564, doi:10.1175/MWR3466.1.

Table 1: Statistical measures of model performance for surface and entire water column.

Correlations are shown in bold, relative standard deviation (model/observed) in regular type,

RMS error in italics and mean bias underlined.

	CORE (**Corr**, RSD, *RMSE*, Bias)	ESM2.1 (**Corr**,RSD, *RMSE*, Bias)
SST	**0.998**, 0.989, *0.84*, -0.50	**0.99**,0.92,*1.43*, -0.08
SSS	**0.98**,1.01,*0.38*,0.18	**0.88**,1.04,*0.85*, -0.15
Surf PO4 (80S-70N)	**0.96**, 0.97,*0.18*,0.033	**0.91**, 0.96, *0.24*, -0.037
Surf NO3 (80S-70N)	**0.97**, 0.99,*2.32*, -0.26	**0.94**,0.86,*3.18*, -0.73
Ln(chl) 70S-70N	**0.73**,1.11,*0.29*, -0.08	**0.72**,0.83,*0.25*, -0.09
Temp (3D)	**0.99**,1.02,*0.82*,0.31	**0.98,**0.96,*1.21*, 0.84
Salt (3D)	**0.94**,1.10,*0.18*, -0.001	**0.92**,1.13,*0.20*, -0.001
PO4 (3D)	**0.93**,1.05,*0.23*,0.00	**0.84**,1.13,*0.39*,0.00
NO3 (3D)	**0.83**, 1.05. *5.7*, -2.0	**0.76**, 0.89,*7.7*,-4.7

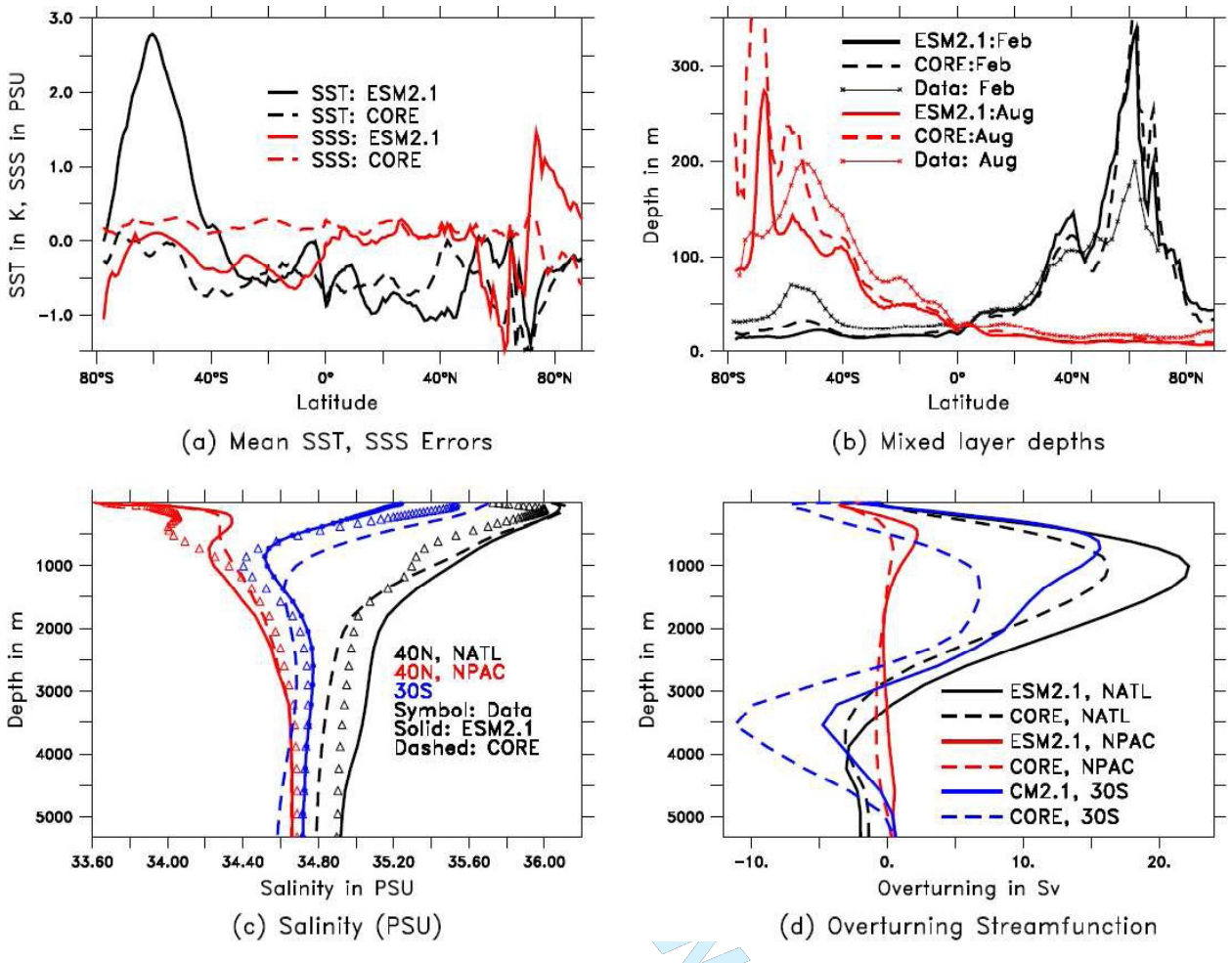

Figure 1: Evaluation of the physical circulation in the ESM2.1 (thick solid lines) and CORE (thick dashed lines). (a) Zonally and annually averaged surface temperature biases. (b) Zonally averaged February (black) and August (red) mixed layer depths. Averaged mixed layer depth from de Boyer Montegut et al. (2007) shown with the thin line and symbols. (c) Zonally averaged profiles of salinity at 40N in the North Atlantic (black), 40N in the North Pacific (red) and 30S across the entire Southern Ocean (blue). (d) Overturning streamfunction at 40N in the North Atlantic (black), 40N in the North Pacific (red) and 30S in the Southern Ocean (blue).

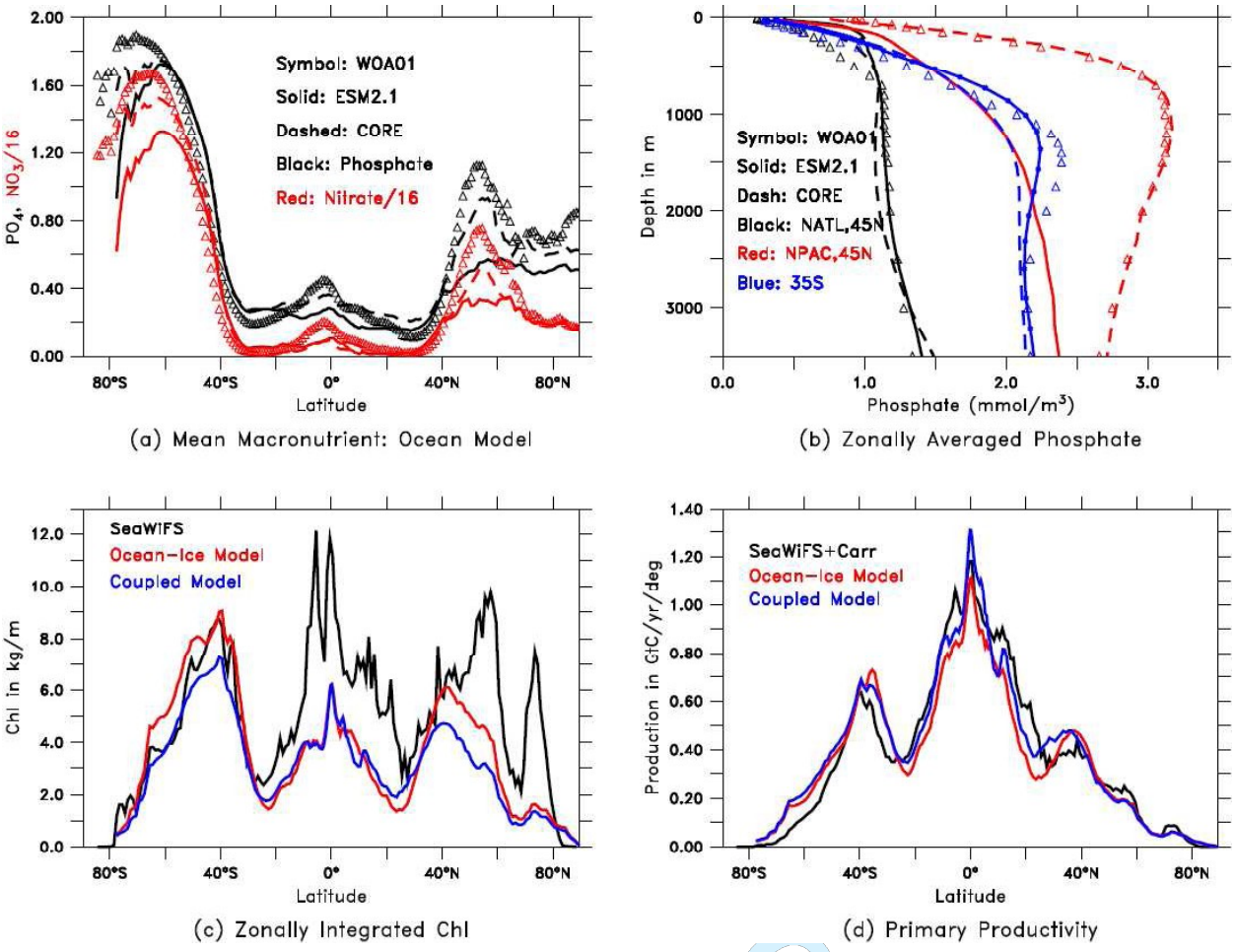

Figure 2: Evaluation of model fidelity. (a) Annual mean surface phosphate (black) and nitrate/16 (red) from data (WOA01, Conkright et al., 2002, symbols), ESM2.1 (solid lines) and CORE (dashed lines). (b) Zonally averaged phosphate over the top 1500m. Symbols are data, black lines an average within the North Atlantic, red lines an average within the North Pacific and blue lines an average across the Southern Ocean. (c) Zonally integrated chlorophyll the SeaWiFS satellite (black) compared with surface chlorophyll from the models. (d) Primary productivity compared with that estimated from the SeaWiFS satellite using the algorithm of Carr (2002).

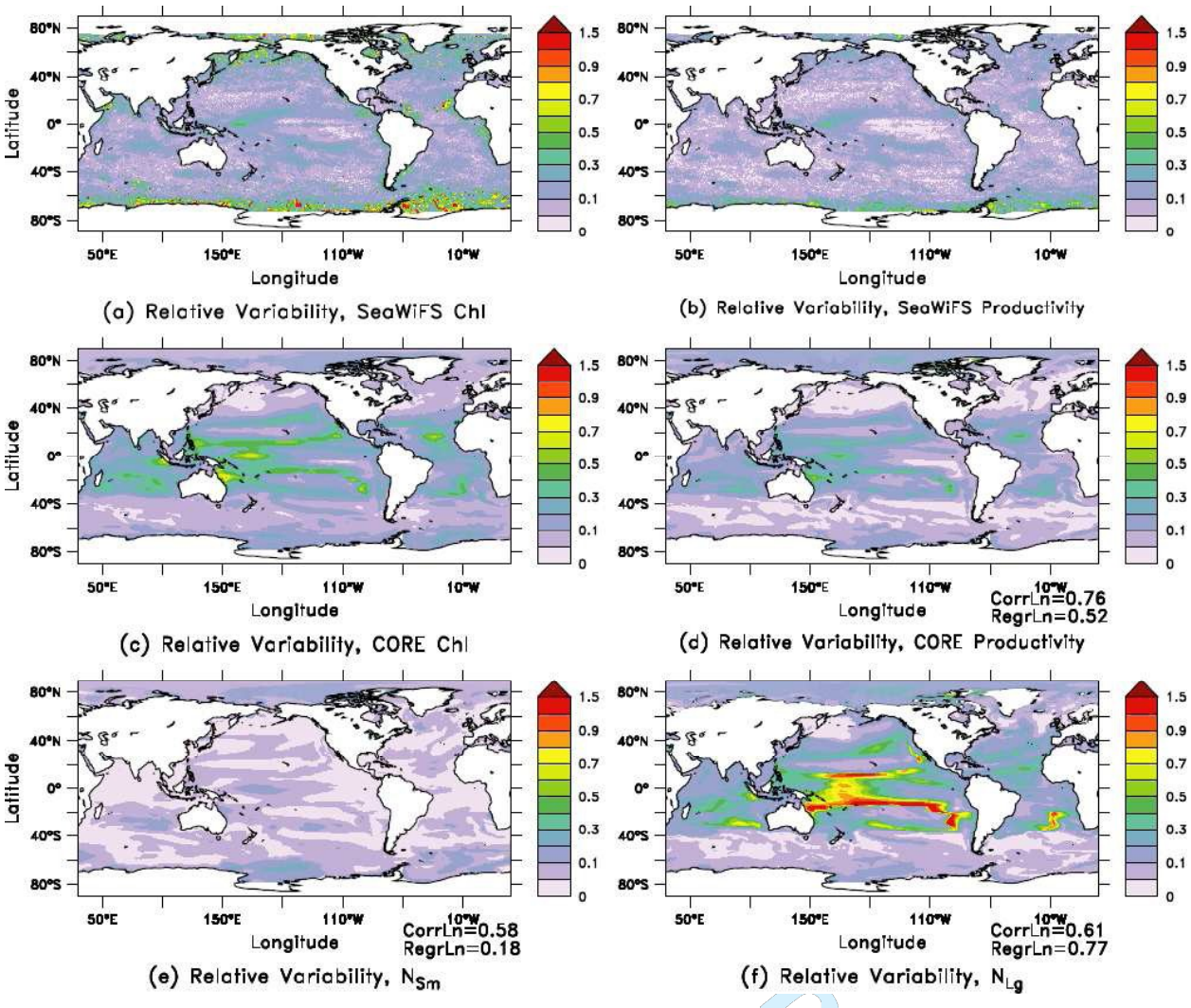

Figure 3: Coefficients of variability (standard deviation of 12-month running smoothed/mean) for quantities estimated from satellite and computed in a CORE-forced (Griffies et al. 2009) ocean-ice model. Contours are 0,0.05, 0.1 to 1 by 0.1, and 1.5. Correlations and regressions between the natural log of chlorophyll and the natural log of the relevant quantity are shown to give a sense of power law relationships for the model output. (a) Surface chlorophyll, SeaWiFS. (b) Primary productivity from SeaWiFS using the Carr (2002) algorithm. (c) Surface chlorophyll from the model. (d) Productivity (total grazing 0-100m). (e) Small phytoplankton biomass 0-100m. (f) Large phytoplankton biomass 0-100m.

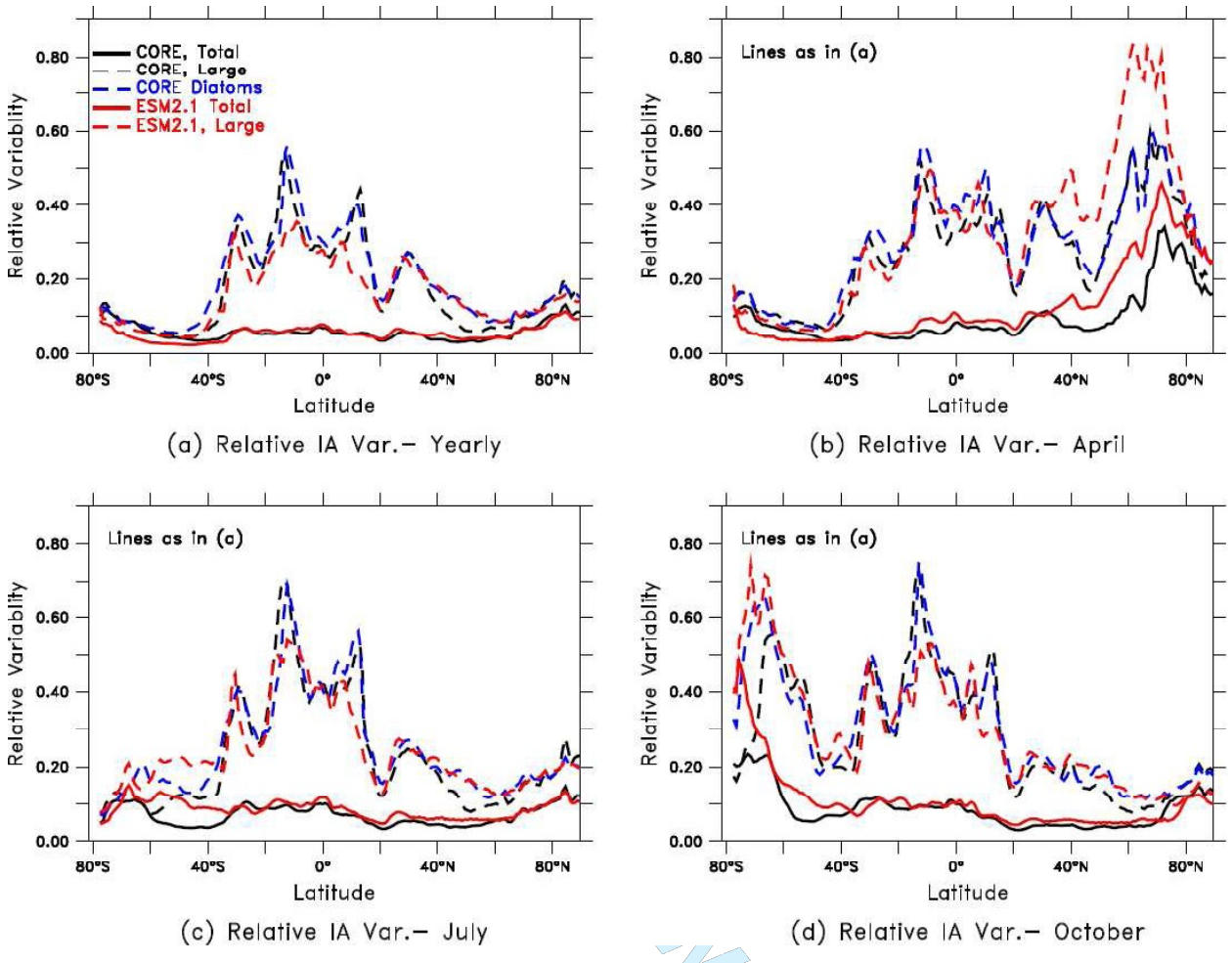

Figure 4: Zonally averaged coefficient of variation of phytoplankton biomass (standard deviation/mean) as a function of space and time. Red lines are for years 401-500 of ESM2.1, black lines for the CORE forced run. Solid lines are for total phytoplankton biomass, while dotted lines are for large phytoplankton biomass alone. (a) Variability of 12-month smoothed biomass. (b) Same as (a) but only for the month of April. (c) Same as (a) but only for the month of July. (d) Same as (a) but only for the month of October.

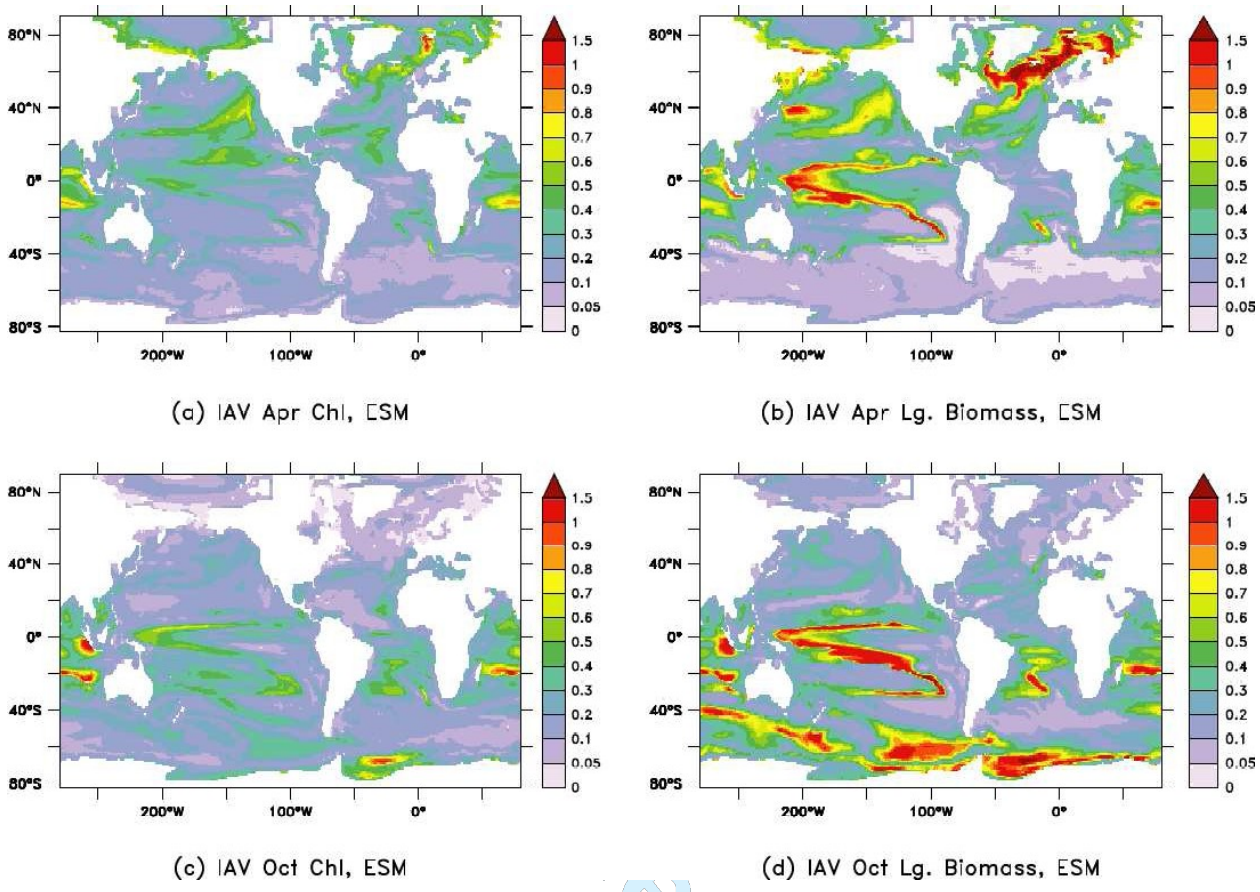

Figure 5: Interannual variability in spring/fall for the Earth System model. All plots show standard deviation over mean. (a) Surface chlorophyll, April. (b) Large phytoplankton biomass, April. (c) Surface chlorophyll, October. (d) Large phytoplankton biomass, October.

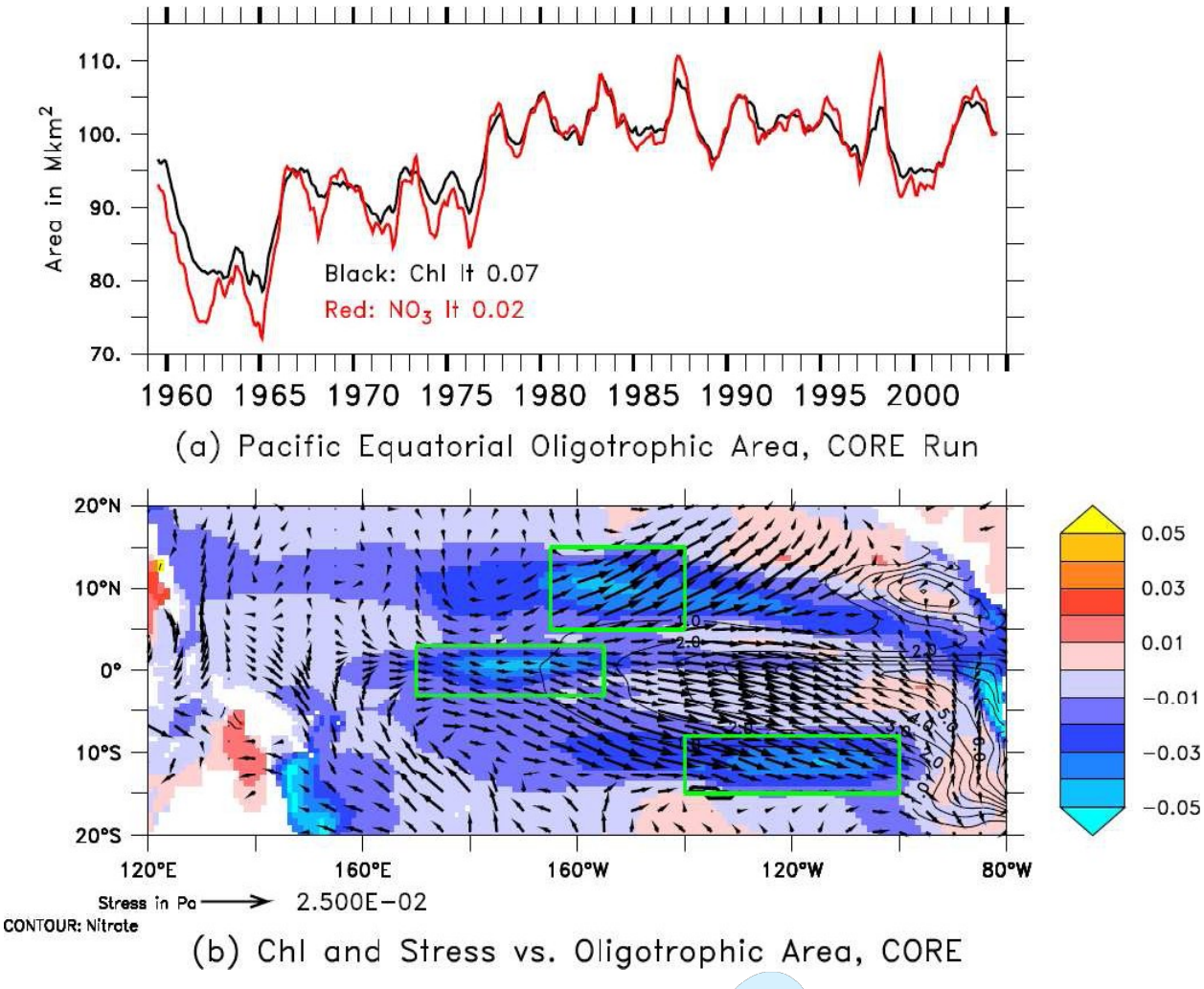

Figure 6: Changes in oligotrophic gyre area in the Central Pacific (20N-20S, following definition of Polovina et al, 2008). (a) Changes in the oligotrophic gyre area in the CORE forced model. (b) Changes in surface chlorophyll (colors) and on wind stress (vectors) corresponding to a 1 standard deviation change in gyre area.

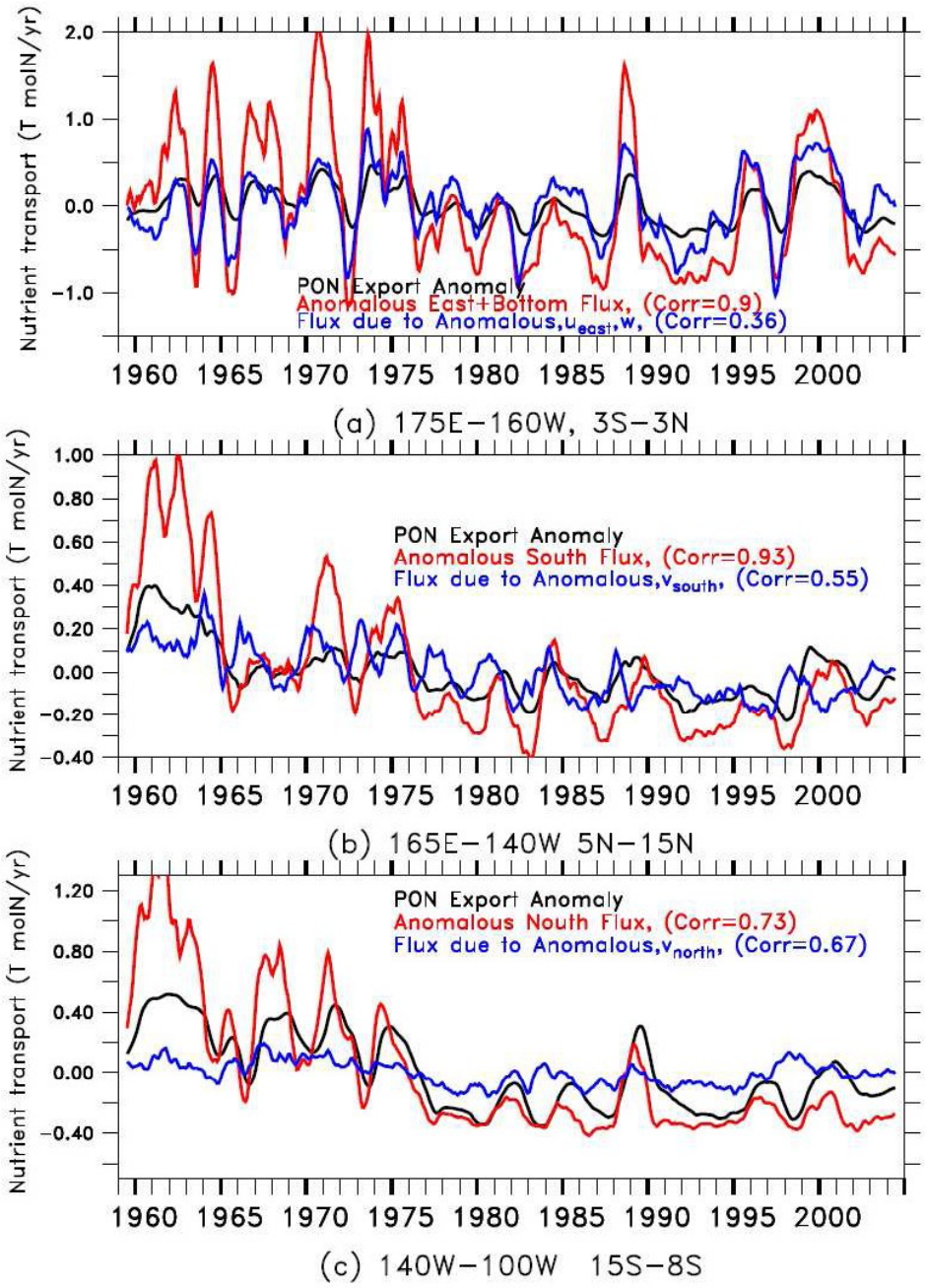

Figure 7: Time series of anomalous export of particulate organic nitrogen (black lines), advective fluxes of nitrate (red lines) and advective fluxes due to changes in velocity alone (blue lines) for the three centers of action in Figure 7. (a) 175E-160W, 3S-3N. (b) 160W-140W, 5N-15N. (c) 140W-100W, 15S-8S.

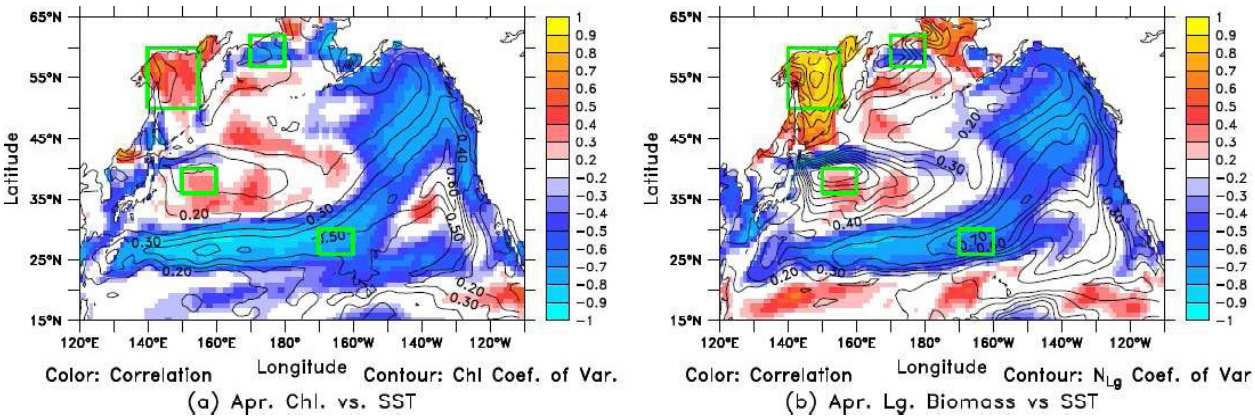

Figure 8: Relationship of variability in local sea surface temperature with variability in (a) chlorophyll and (b) large phytoplankton biomass during the month of April in the North Pacific. Colors show correlation coefficients, contours the interannual variability normalized by the mean as in Figure 5.

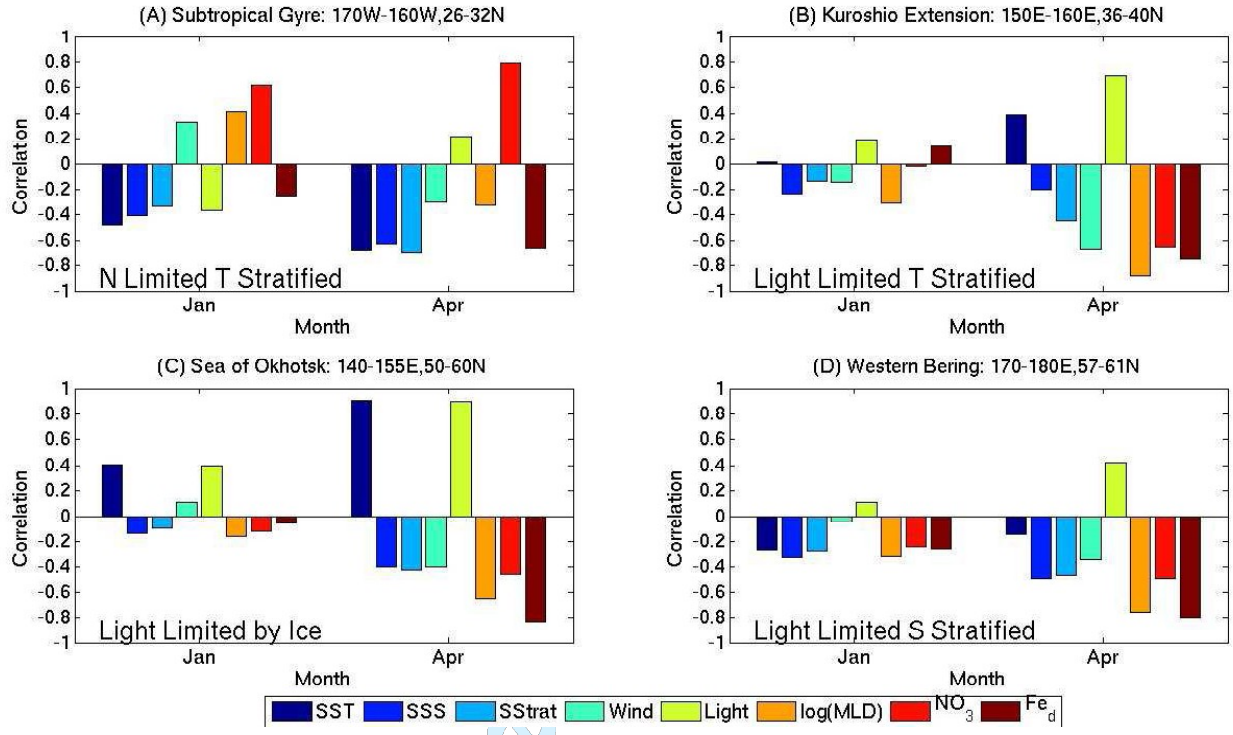

Figure 9: Large phytoplankton biomass during April correlated with other fields at two months (January and April) in the four different dynamical regimes in the North Pacific denoted by the green boxes in Figure 8. (a) Subtropical gyre, 170W-160W, 26N-30N. Dominant correlation is with nitrate both at 0 lag and with a three month lead, consistent with stronger wintertime convection and southward advection of nitrate driving variability. (b) Kuroshio extension region, 150E-160E, 36N-40N. Strong correlation with light, anticorrelation with mixed layer depth at zero lag, little correlation at three month lead, consistent with shallowing of mixed layer playing dominant role. Anticorrelation with wind suggests that weak winds are important in modulating mixed layer depths in this region. (c) Sea of Okhotsk. Highest correlation at zero lag with mixed layer light and temperature, consistent with variation in sea ice cover playing dominant role. (d) Western Bering sea. Strong anticorrelation with mixed layer depth, positive correlation with light. Consistent with a light-limited, salinity stratified regime.